ULTRASOUND ELASTOGRAPHY: DEEP LEARNING APPROACH

Md Golam Kibria

A thesis

in

The Department

of

Electrical and Computer Engineering

Presented in Partial Fulfillment of the Requirements

For the Degree of Master of Applied Science

Concordia University

Montréal, Québec, Canada

February 2021

Concordia University

School of Graduate Studies

This is to certify that the thesis prepared

By: **Md Golam Kibria**

Entitled: **Ultrasound Elastography: Deep Learning Approach**

and submitted in partial fulfillment of the requirements for the degree of

Master of Applied Science

complies with the regulations of this University and meets the accepted standards with respect to originality and quality.

Signed by the final examining commitee:

Dr. Wahab Hamou-Lhadj _____ Chair, Examiner

Dr. Fuzhan Nasiri _____ Examiner, External

Dr. Hassan Rivaz _____ Supervisor

Dr. Andreas Bergdahl _____ Co-supervisor

Approved _____

Dr. Yousef R. Shayan, Chair

Department of Electrical and Computer Engineering

February 2021 _____

Dr. Mourad Debbabi, Interim Dean

Gina Cody School of Engineering and Computer Science

Abstract

Ultrasound Elastography: Deep Learning Approach

Md Golam Kibria

Ultrasound elastography images the elasticity of a biological tissue. Conventional algorithms for ultrasound elastography suffer from different noises severely compromising the quality of time-delay estimation. Calculation of time-delay estimation is a key component of strain estimation. However, time-delay estimation is analogous to optical flow estimation, a classical computer vision problem. Deep learning networks have reported recent success in optical flow estimation compared to the conventional techniques. Classical ultrasound elastography algorithms have been unable to provide a single solution to both commonly known issues of noise and computation time. Deep learning techniques have a bright prospect in addressing both issues. The goal of this thesis is to investigate whether optical flow estimation is translatable to ultrasound elastography as the core nature of both of these problems are analogous. In this thesis we aim to develop and train a robust deep neural network for ultrasound elastography. First, an efficient deep learning network trained for optical flow estimation is used for time-delay estimation. The initial time-delay estimation is further fine-tuned by optimizing a global cost function for generating high quality strain images. Simulation, phantom and clinical experiments show the robustness of the deep learning approach both quantitatively and qualitatively. Next, the weights of the deep learning network are fine-tuned using transfer learning technique for transferring the efficacy of optical flow estimation to

time-delay estimation. The objective is to retain the robustness introduced by the deep learning network while enhancing the overall performance of the time-delay estimation in ultrasound elastography. Simulation and experimental phantom results show that the time-delay estimation has improved slightly after fine-tuning the weights using transfer learning.

Acknowledgments

First and foremost, I would like to take this opportunity to thank the Almighty for keeping me and my family safe and secure in the COVID-19 pandemic of 2020 and bestowing me the strength to endure the ordeal with grace and dignity.

I would like to express my gratitude to my supervisors Dr. Hassan Rivaz and Dr. Andreas Bergdahl for their steadfast support and direction. I appreciate the guidance and financial support they have provided. I am grateful for their constant guidance and encouragement.

I am thankful to all the brilliant minds at IMPACT lab for sharing their enriched insights during lab meetings and group discussions. I am very much grateful to Professor Hassan Rivaz, the director of IMPACT lab. It has been a rewarding experience to work with Professor Rivaz who has been an excellent mentor to me, providing me with encouragement and guiding me throughout my studies. He has been a constant support during difficult times. I would like to show my gratitude to Dr. Rupert Brooks for sharing his extensive knowledge and expertise about deep learning. His amazing ability for explaining complex aspects of deep learning has been vital to this work.

I would like to thank Drs. E. Boctor, M. Choti and G. Hager for their permission to use the *in-vivo* liver data. I would like to acknowledge that this work has been supported in part by the Natural Sciences and Engineering Research Council of Canada (NSERC) RGPIN-2020-04612.

I would like to express my appreciation to my thesis committee members Drs. Wahab Hamou-Lhadj, Fuzhan Nasiri, Andreas Bergdahl and Hassan Rivaz for their constructive remarks and valuable insights.

I would like to appreciate the valuable and enriching discussions with my friends and colleagues Ali Kafaee, Bahareh Behboodi, Md Ashikuzzaman, Morteza Mirzaei, Mumu Aktar, Sobhan Goudarzi and Clyde Belasso in different stages of my study. I would also like to thank Thomas Beaudry for his technical support.

Finally, I would like to express my ultimate gratitude towards my family for their unconditional and unwavering support. I enormously grateful to my eldest brother, Md Golam Mostofa, for believing in me through all the ups and downs. I would like to offer my undiluted gratitude towards my beloved wife, Lutfun Nahar, for her love, patience and non-stop caring.

Contents

List of Figures

List of Tables

Chapter 1

Introduction

As a medical imaging modality, ultrasound is non-invasive, portable and provides results in real-time which increases its pragmatic importance in clinical diagnosis. Among many other applications of ultrasound imaging technology, this thesis focuses on speckle tracking, displacement estimation of biological tissue and elastography.

1.1 Ultrasound Physics

Ultrasound medical imaging scanners uses acoustic waves for scanning. Although any sound wave with a frequency above 20kHz is considered ultrasonic, clinical devices typically use frequencies between 1-20 MHz.

The sonographic scanner primarily consists of two units, the transducer and the processing unit. The transducer emits acoustic pulses towards the targeted tissue and receives back the reflected and back-scattered pulses. It consists of an array of piezoelectric sensors that can emit acoustic pulses with variable frequency and length upon being subjected to proper electrical signals. The emitted acoustic pulses penetrate the skin and the underlying biological tissues. The acoustic

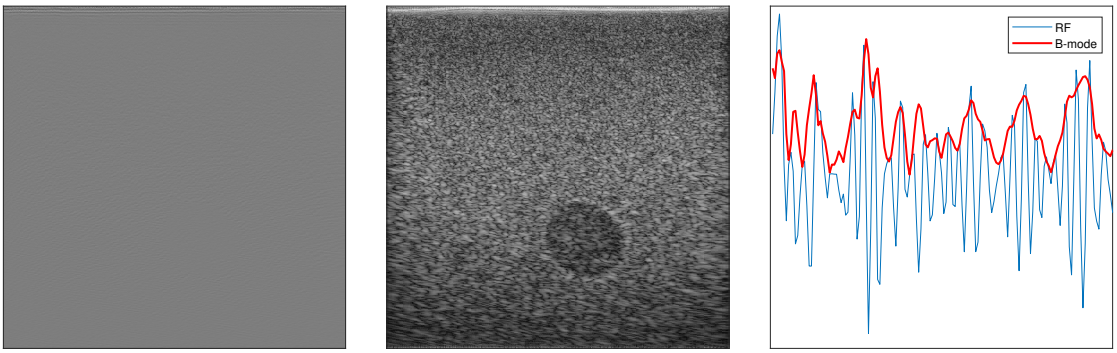

(a) RF frame (b) B-Mode (c) RF vs B-mode Signal

Figure 1: ((a) RF frame and (b) B-mode image of an ultrasound scan of a CIRS breast phantom. (c) RF and B-mode signal plot of a portion of an axial line of the same ultrasound scan)

waves travel through many layers of different type of biological tissue which act as different acoustic mediums. While travelling, the waves get impeded by many scatterers. As a result, a portion of the acoustic energy gets absorbed and scattered, and the rest is reflected towards the transducer. The acoustic energy of the reflected wave depends on the physical property of the scatterers. In a sense, the reflected energy signature of the waves represents the properties of the scatterers. This way it is possible to extract information on many physical properties of the biological tissue using ultrasound such as speckle size, blood-flow, elasticity and characteristic of a tumor.

The data obtained by the transducer goes through different levels of processing. Most researchers are interested in Radio Frequency (RF) data while most clinical practice involves with B-mode ultrasound image. B-mode image is obtained through envelop detection and log compression of RF data and is rather visually useful than RF data for clinical diagnosis. The lesion of the CIRS breast phantom is more clearly visible in B-mode image than in RF image (Fig. 1). Nevertheless, useful information can be extracted from RF data. Compared to B-mode data, RF data is less exposed to processing which gives the research community more

room for experimenting.

1.2 Ultrasound Elastography

Ultrasound elastography [1] medical imaging technique entails calculating the elastic properties of different organs of human body such as prostate [2, 3], liver [4–11], thyroid [12] and breast [13–19]. Ultrasound elastography is mainly two types; "dynamic" and "quasi-static". Dynamic ultrasound elastography involves generating palpation of the tissue by using acoustic force. Shear-wave elastography [20–22] and acoustic radiation force imaging (ARFI) [23] are prime examples of dynamic ultrasound elastography. On other hand, quasi-static ultrasound elastography such as free hand palpation ultrasound elastography [15, 24] introduces tissue deformation by external force, generally using hand-held probe. This thesis is primarily focused on quasi-static elastography algorithms which can be widely categorized into three groups; classical, regularized, and deep learning ultrasound elastography.

1.2.1 Classical Ultrasound Elastography

Most classical algorithms approach ultrasound elastography from a physical point of view where each RF frame corresponds to a cross-section of the scanned tissue. The RF frame can be divided into small windows which correspond to small patches of the physical tissue. These window-based techniques [15, 16, 25–28] take two corresponding pre- and post- deformation RF frame and conduct block-matching search using predefined corresponding windows to track down the displacements. The block matching techniques used are either cross-correlation based [1, 29, 30] or phase-root seeking based [28, 31]. Most of these window-based methods calculate time-delay estimation (TDE) which is spatially differentiated to obtain the strain

image using the least-squares [32] or gradient-based methods. TDE is estimated either in axial direction [1, 33] or in both axial and lateral direction [34, 35]. Displacement estimation in lateral direction is much less accurate than in axial direction. Data sampling rate in lateral direction is significantly lower [36, 37] than axial direction which is why ultrasound RF signals show wider point spread function (PSF) [38].

Another group of window-based elastography algorithms [39–41] skip the displacement estimation and directly estimates strain. In ideal condition, the post-compression RF window can be stretched by a factor when it becomes identical to pre-compression window. The direct strain estimators find the desired stretching factor using adaptive temporal stretching locally or globally both in time-domain [39] and in spectral-domain [40, 41]. These approaches are computationally expensive because of the exhaustive search. But as displacement estimation is bypassed for direct strain estimation, gradient noise can be avoided. Phased-based approaches operate in spectral domain and are generally computationally efficient [42, 43]. Phase-root seeking method looks for the phase-root of the zero-lagged cross-correlation of the corresponding analytic pre- and post-compression windows [43]. On the downside of the phase-root seeking method, an error in the displacement estimation can propagate further down the axial line. As a result, this approach becomes more susceptible to decorrelation noise. To overcome this Pesavento *et al.* [44] proposed an additional stretching of the post-compression temporal window with lateral displacement correction before phase-root seeking which is computationally expensive. Shiina *et al.* [45] proposed a method where phase is calculated at the top of autocorrelation envelop for axial and lateral displacement estimation. Lindop *et al.* [46] proposed a phase-based algorithm, known as weighted phase separation (WPS) which estimates displacement along with its location. Brusseau *et al.* [47] proposed a

phase-based direct strain estimation method which involves exhaustive search of stretching factor with adaptive window length and position.

Another group of elastography algorithms take a kernel-based approach [25, 31, 48, 49] where effects of neighboring windows are considered through exponential weighted averaging. These methods operate both in time-domain [48] and spectral-domain [31, 49]. They gain some advantage over decorrelation noise for kernel-based approach at the cost of overhead computation of neighboring windows.

Other noteworthy works in classical ultrasound elastography include using Bayesian optimization techniques [50–53], beam-steered [54] and volumetric ultrasound data [10, 55–58].

1.2.2 Regularization Ultrasound Elastography

Regularization-based ultrasound elastography techniques calculates TDE by optimizing a cost function [5, 59–61] which integrates RF signal correspondence between pre- and post- deformation frames with displacement continuity. The cost function contains data similarity term which incorporates RF signal correspondence and regularization term which ensure displacement continuity constraint is satisfied. Optimization of the cost function yields a spatially smooth displacement map but the process is computationally taxing which is resolved by deploying dynamic programming (DP) technique [60, 62]. DP yields integer values field which is inadequate for accurate and spatially smooth displacement map. DP estimates is further refined by Dynamic Programming Analytic Minimization (DPAM) [5]. DPAM shows striking artifacts vertically along scan lines due to discontinuity of displacement location between two adjacent scan lines in lateral direction. To overcome this issue, Global Ultrasound Elastography (GLUE) [63] method considers the entire RF frame into formulating a cost function.

To further improve the quality of displacement estimation, Spatio-Temporal Global Ultrasound Elastography (GUEST) [6] incorporates temporal continuity where three RF frames constitute the cost function. Further fine-tuning is accomplished by incorporating total variation regularization technique [64] and principal component analysis [65].

1.2.3 Deep Learning Ultrasound Elastography

Deep learning algorithms have gained much popularity for image processing, image classification and segmentation. The adaptive learning nature of deep learning techniques holds a certain attraction for ultrasound elastography where the classical algorithms face many sources of noise. The classical approaches failed to provide a single solution to all the problems associated with ultrasound elastography. The gradual training of deep learning framework promises a robust solution to ultrasound elastography addressing both issues of noise and computation time. As a result, there has been a recent explosion of deploying deep learning in ultrasound elastography.

1.2.3.1 Deep Learning and Convolutional Neural Network

In artificial intelligence, machine learning algorithms can recognize patterns in vast amounts of data that would take years for humans to detect. These pattern detection capabilities can help in decision making in many practical situations. Deep learning is a branch of machine learning which deals with both unstructured and unlabeled data sets. Deep learning uses an array of interconnected nodes to create a network and learn pattern detection and decision making in a way human brain operates. The nodes of the network are typically compared with the neuron, the unit cell structure of the human brain. Hence the network of nodes associated with deep learning is widely known as neural network. A typical neural network

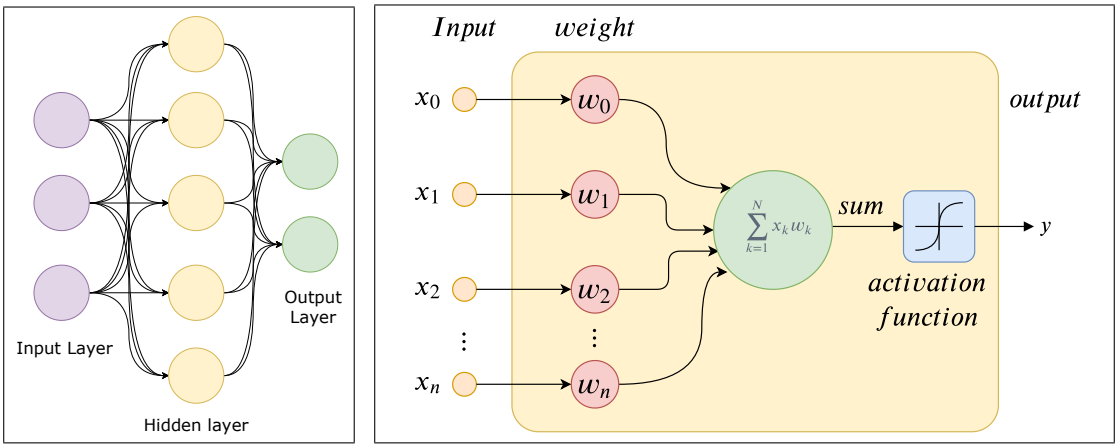

(a) Neural Network (b) Artificial Neuron

Figure 2: (a) A typical neural network (b) Structure of a typical artificial neuron of neural network

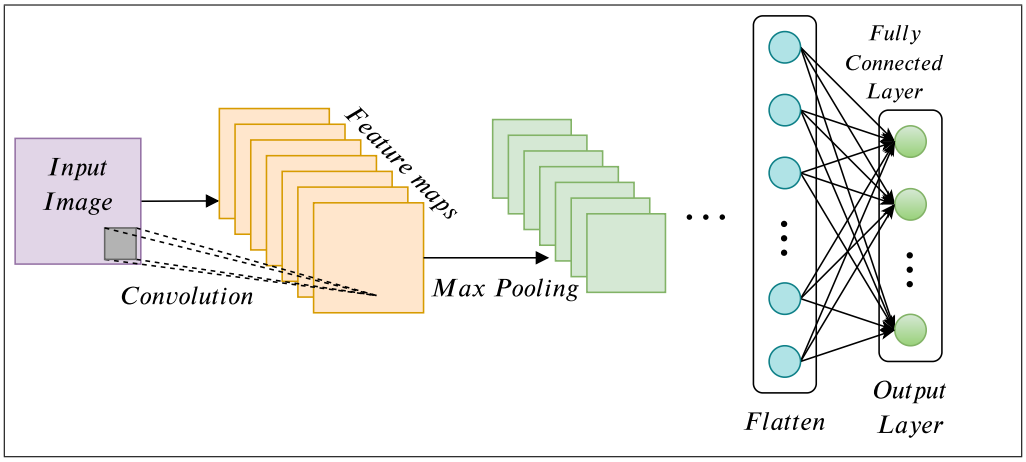

Figure 3: Cartoon illustration of a typical Convolutional Neural Network

consists of an input layer at the left, the output layer at the right and one or more hidden layers in the middle (Fig. 2(a)). Normally nodes of adjacent layers are interconnected while nodes within a layer are not connected. Each node acts as a mathematical unit where inputs are multiplied by weights and their summation go through an activation function (Fig. 2(b)).

Convolutional Neural Network (CNN) is a special kind of neural network that can handle image data with ease. Most CNNs are trained for image classification where the network learns to classify images into different designated categories.

CNNs also deal with problems related with per-pixel prediction such as semantic segmentation, augmented reality and optical flow estimation for applications like object detection and automated driving. CNNs takes images as input, extract useful feature from them using convolution filters. Unlike neural networks, the weights of the kernels of the convolution layer is shared throughout the whole image. This way each kernel in a convolution layer learns to extract a unique feature from the input, also known as feature maps. Unlike conventional filters in image processing, weights of the kernels of a CNN layer are not hand-engineered but learned through extensive training with ample amount of data. Normally, deep CNNs are comprised of several convolution layers. There are maxpool layers in between convolution layers which reduce the dimension of the feature maps by a certain predefined factor. The deeper the input data travels into the network, the data is reduced more in width and height due to maxpool operation. At the very end the feature maps are flattened followed by a fully connected layer and output. Fully convolutional network does not have fully connected layer which makes it possible to take input of arbitrary size.

1.2.3.2 Machine Learning in Ultrasound Elastography

Displacement estimation from corresponding ultrasound scans suffers greatly from many sources of noise such as decorrelation noise, jitter noise etc. compromising the quality of the strain images obtained from the displacement field. In an attempt to reduce the effect of decorrelation noise on displacement estimation, several methods have been tried over the years. Most prominent of them is the incorporation of the data from neighbourhood pixels/windows into the algorithm. Amidabadi *et al.* [66] incorporated this idea with machine learning technique support vector machine (SVM) to extract useful features from the neighbourhood pixels in order to reduce the peak-hopping error and ultimately improving the

overall quality of the strain image produced by the underlined elastography algorithm.

Recently there has been some notable contemporary works on ultrasound elastography in deep learning domain such as implicit strain reconstruction using end-to-end convolutional neural network [67,68]. An important aspect of obtaining quality strain image is the selection of best-suited frame which has been automated in [69]. Peng *et al.* [70] investigated the efficacy of present deep learning networks for optical flow estimation such as FlowNet 2.0 [71], PWC-Net [72] and LiteFlow-Net [73] by using transfer learning techniques. Tehrani *et al.* [74] has proposed two deep networks MPWC-Net and RFMPWC-Net where multi-level pyramid warping and cost volume network has been exploited for ultrasound elastography.

1.3 Objective of the Thesis

Displacement estimation in ultrasound elastography is very analogous to optical flow estimation. Recently, deep CNNs have gained promising success in optical flow estimation. Dosovitskiy *et al.* [75] first proposed two CNN architectures namely, FlowNetS (short for FlowNet-Simple) and FlowNetC (short for FlowNet-Correlation), which gained competitive visual and quantitative accuracy in optical flow estimation compared to the state-of-the-art conventional methods while achieving real-time execution time. Ilg *et al.* [71] further improved the networks by suggesting a specific training schedules and also experimented on stacking the networks on top of each other. Finally, a new architecture FlowNet 2.0 [71] was proposed where a combination of FlowNetC and FlowNetS stacked together and trained with a specific schedule. Surprisingly, FlowNet 2.0 achieved much better result than its previous counterparts FlowNetC and FlowNetS while

performing in real-time.

The overwhelming success of CNN architectures in optical flow estimation has paved the way for exploring the possibilities of this exciting field of machine learning in ultrasound elastography. In this thesis, we explored the possibility of using convolutional neural network for ultrasound elastography. At first, we checked the performance of the FlowNet 2.0 architecture with ultrasound RF data. By using the trained weights by [71], we found that FlowNet 2.0 can generate a coarse displacement field which needed further refinement for generating quality strain image. Therefore, we used global optimization based ultrasound elastography technique GLUE [63] for further refining the coarse displacement generated by FlowNet 2.0. The fact that FlowNet 2.0 can generate coarse displacement field from ultrasound RF data is a clear indicator that convolutional neural network can be successfully used for ultrasound elastography and speckle tracking. Eventually we aimed at fine-tuning FlowNet 2.0 network weights with ultrasound RF data using transfer learning techniques for improving the coarse displacement estimation from FlowNet 2.0 in order to generate quality strain image.

1.4 Organization of the Thesis

In Chapter 2 we propose a robust deep neural network based ultrasound elastography method GLUENet where we get coarse and robust displacement estimation from FlowNet 2.0 network and further fine-tune it by a global optimization based method GLUE for better strain estimation. Simulation, experimental and clinical results show the superior performance of our method. In Chapter 3 we propose fine-tuning the already trained weights of FlowNet 2.0 network model using transfer learning technique improving its performance

on displacement estimation. The estimated strain profile calculated from the displacement estimation obtained from fine-tuned FlowNet 2.0 was not up to satisfactory level. One of the reasons behind this non-satisfactory performance of transfer learning may be the complex network structure and training schedule of FlowNet 2.0. Simulation and experimental phantom results show slight improvement of displacement estimation for fine-tuning FlowNet 2.0. We draw concluding remark and mention possible future work in Chapter 4.

Chapter 2

GLUENet: Ultrasound Elastography Using Convolutional Neural Network

This chapter is published in the conference paper below, which according to our best knowledge, is the first published work that exploited deep learning in ultrasound elastography. The paper is cited 21 times according to Google Scholar.
Kibria, Md Golam, and Hassan Rivaz. "Gluenet: Ultrasound elastography using convolutional neural network." Simulation, Image Processing, and Ultrasound Systems for Assisted Diagnosis and Navigation. Springer, Cham, 2018. 21-28.
Displacement estimation is a critical step in ultrasound elastography and failing to estimate displacement correctly can result in large errors in strain images. As conventional ultrasound elastography techniques suffer from decorrelation noise, they are prone to fail in estimating displacement between echo signals obtained during tissue deformations. This chapter proposes a novel elastography technique which addresses the decorrelation in estimating displacement field. We call our method GLUENet (GLobal Ultrasound Elastography Network) which uses deep

Convolutional Neural Network (CNN) to get a coarse but robust time-delay estimation between two ultrasound images. This displacement is later used for formulating a nonlinear cost function which incorporates similarity of RF data intensity and prior information of estimated displacement [63]. By optimizing this cost function, we calculate the finer displacement exploiting all the information of all the samples of RF data simultaneously. The coarse displacement estimate generated by CNN is substantially more robust than the Dynamic Programming (DP) technique used in GLUE for finding the coarse displacement estimates. Our results validate that GLUENet outperforms GLUE in simulation, phantom and *in-vivo* experiments.

2.1 Introduction

Ultrasound elastography can provide mechanical properties of tissue in real-time, and as such, has an important role in point-of-care ultrasound. Estimation of tissue deformation is very important in elastography, and further has numerous other applications such as thermal imaging [76] and echocardiography [77].

Over the last two decades, many techniques have been reported for estimating tissue deformation using ultrasound. The most common approach is window-based methods with cross-correlation matching techniques. Some reported these techniques in temporal domain [29,48,78] while others reported in spectral domain [25, 43]. Another notable approach for estimating tissue deformation is usage of dynamic programming with regularization and analytic minimization [5] [63]. All these approaches may fail when severe decorrelation noise exists between ultrasound images.

Tissue deformation estimation in ultrasound images is an analogous to the optical flow estimation problem in computer vision. The structure and elastic property

of tissue impose the fact that tissue deformation must contain some degree of continuity. Hence, tissue deformation estimation can be considered as a special case of optical flow estimation which is not bound by structural continuity. Apart from many state-of-the-art conventional approaches for optical flow estimation, very recently notable success has been reported at using deep learning network for end-to-end optical flow estimation. Deep learning networks enjoy the benefit of very fast calculation by trained (fine-tuned) weights of the network while having a trade-off of long-time computationally exhaustive training phase. Deep learning has been recently applied to estimation of elasticity from displacement data [79]. A promising recent network called FlowNet 2.0 [71] has achieved up to 140 fps at optical flow estimation. These facts indicate the potential for using deep learning for tissue deformation estimation.

This work takes advantage of the fast FlowNet 2.0 architecture to estimate an initial time delay estimation which is robust from decorrelation noise. This initial estimation is then fine-tuned by optimizing a global cost function [63]. We call our method GLUENet (GLobal Ultrasound Elastography Network) and show that it has many advantages over conventional methods. The most important one would be the robustness of the method to severe decorrelation noise between ultrasound images.

2.2 Methods

The proposed method calculates the time delay between two radio-frequency (RF) ultrasound scans which are correlated by a displacement field in two phases combining fast and robust convolutional neural network with the more accurate global optimization based coarse to fine displacement estimation. This combination is possible due to the fact that the global optimization-based method

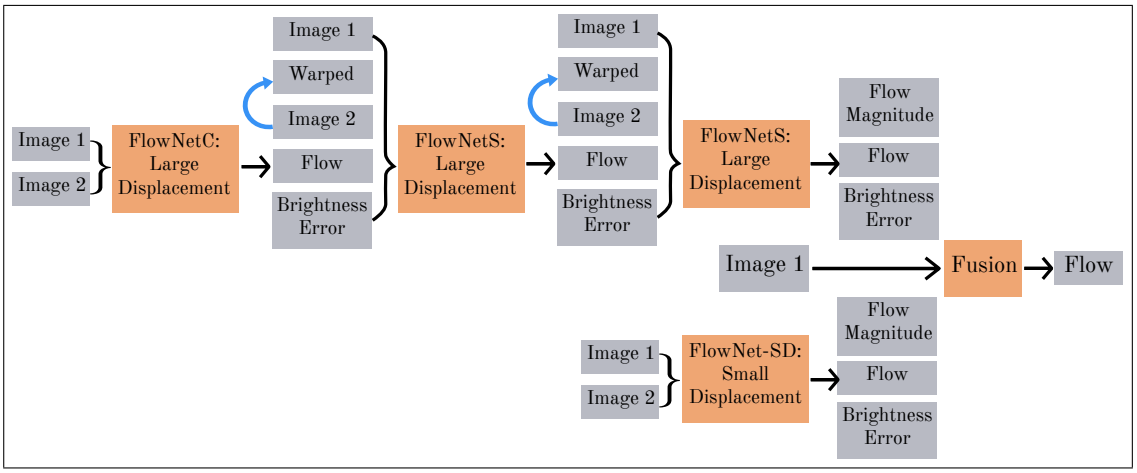

Figure 4: Full schematic of FlowNet 2.0 architecture: The initial network input is Image 1 and Image 2. The input of the subsequent networks includes the image pairs, previously estimated flow, Image 2 warped with the flow, and residual of Image 1 and warped image (Brightness error). Input data is concatenated (indicated by braces).

depends on coarse but robust displacement estimation which CNN can provide readily and more robustly than any other state-of-the-art elastography method.

Optical flow estimation in computer vision and tissue displacement estimation in ultrasound elastography share common challenges. Therefore, optical flow estimation techniques can be used for tissue displacement estimation for ultrasound elastography. The latest CNN that can estimate optical flow with competitive accuracy with the state-of-the-art conventional methods is called FlowNet 2.0 [71]. This network is an improved version of its predecessor FlowNet [75], wherein Dosovitskiy *et al.* trained two basic networks namely FlowNetS and FlowNetC for optical flow prediction. FlowNetC is a customized network for optical flow estimation whereas FlowNetS is rather a generic network. The details of these networks can be found in [75]. These networks were further improved for more accuracy in [71] which is known as FlowNet 2.0.

Fig. 4 illustrates the complete schematic of FlowNet 2.0 architecture. It can be considered as the stacked version of a combination of FlowNetC and FlowNetS

architectures which help the network to calculate large displacement optical flow. For dealing with the small displacements, small strides were introduced in the beginning of the FlownetS architecture. In addition to that, convolution layers were introduced between upconvolutions for smoothing. Finally, the final flow is estimated using a fusion network. The details can be found in [71].

The displacement estimation from FlowNet 2.0 is robust but needs more refinement in order to produce strain images of high quality. Global Time-Delay Estimation (GLUE) [63] is an accurate displacement estimation method provided that an initial coarse displacement estimation is available. If the initial displacement estimation contains large errors, then GLUE may fail to produce accurate fine displacement estimation. GLUE refines the initial displacement estimation by optimizing a cost function incorporating both amplitude similarity and displacement continuity. It is noteworthy that the cost function is formulated for the entire image unlike its motivational previous work [5] where only a single RF line is optimized. The details of the cost function and its optimization can be found in [63]. After displacement refinement, strain image is obtained by using least square or a Kalman filter [5].

2.3 Results

GLUENet is evaluated using simulation and experimental phantom, and *in-vivo* patient data. The simulation phantom contains a soft inclusion in the middle and the corresponding displacement is calculated using Finite Element Method (FEM) by ABAQUS Software (Providence, RI). For ultrasound simulation, the Field II software package [80] is used. A CIRS breast phantom (Norfolk, VA) is used as the experimental phantom. RF data is acquired using an Antares Siemens system (Issaquah, WA) at the center frequency of 6.67 MHz with a VF10-5 linear array at a

sampling rate of 40 MHz. For clinical study, we used *in-vivo* data of three patients. These patients were undergoing open surgical RF thermal ablation for primary or secondary liver cancer. The *in-vivo* data were collected at John Hopkins Hospital. Details of the data acquisition are available in [5]. For comparison of the robustness of our method, we use mathematical metrics such as Mean Structural Similarity Index (MSSIM) [81], Signal to Noise Ratio (SNR) and Contrast to Noise Ratio (CNR). Among them, MSSIM incorporates luminance, contrast, and structural similarity between ground truth and estimated strain images which makes it an excellent indicator of perceived image quality.

2.3.1 Simulation Results

Field II RF data with strains ranging from 0.5% to 7% are simulated, and uniformly distributed random noise with PSNR of 12.7 dB is added to the entire RF data. The additional noise is for illustrating the robustness of the method to decorrelation noise given that simulation does not model out-of-plane motion of the probe, complex biological motion, and electronic noise. Fig. 5 (a) shows ground truth axial strain and (b-c) shows axial strains generated by GLUE and GLUENet respectively at 2% applied strain. Fig. 5 (d-f) illustrates the comparable performance of GLUENet against GLUE [63] in terms of MSSIM, SNR and CNR respectively.

2.3.2 Experimental Phantom Results

Fig. 6 (a-b) shows axial strains of the CIRS phantom generated by GLUE and GLUENet respectively. The large blue and red windows in Fig. 6 (a-b) are used as target and background windows for calculating SNR and CNR (Table 1). The small windows are moved to create a total combination of 120 window pairs (6 as target

Table 1: SNR and CNR of the strain images, and failure rate of GLUE and GLUENet for experimental phantom data and *in-vivo* data of patients 1-3.

	GLUE			GLUENet		
	SNR	CNR	Failure Rate(%)	SNR	CNR	Failure Rate (%)
Phantom	39.0363	12.6588	58.0645	43.4363	15.5291	19.3548
Patient 1	53.9914	22.1641	34.6939	54.7700	27.9264	04.8469
Patient 2	47.5051	22.7523	68.3673	55.9494	25.4911	14.5408
Patient 3	31.2440	07.7831	77.0408	28.6152	19.6954	60.7143

and 20 as background) for calculating CNR values. The histogram of these CNR values is plotted in Fig. 6 (c) to provide a more comprehensive view which shows that GLUENet has a high frequency at high CNR values while GLUE is highly frequent at lower values. The histogram of SNR and CNR values is a much better comparison tool of performance than using any blind location of region of interest for calculating single value of SNR and CNR. It provides a more comprehensive comparison. We test both methods on 62 pre- and post- compression RF signal pairs chosen from 20 RF signals of CIRS phantom for a measure of consistency. The best among the estimated strain images is visually marked to compare with other strain images using Normalized Cross Correlation (NCC). A threshold at 0.6 is used to determine failure rate of the methods (Table 1). GLUENet shows very low failure rate (19.3548%) compared to GLUE (58.0645%) which indicates greater consistency of GLUENet.

2.3.3 Clinical Results

Fig. 7 shows axial strains of patient 1-3 from GLUE and GLUENet and histogram of CNR values. Similar to experimental phantom data, small target and background windows are moved to create a total combination of 120 window pairs for calculating CNR values. Their histogram shows that GLUENet has a

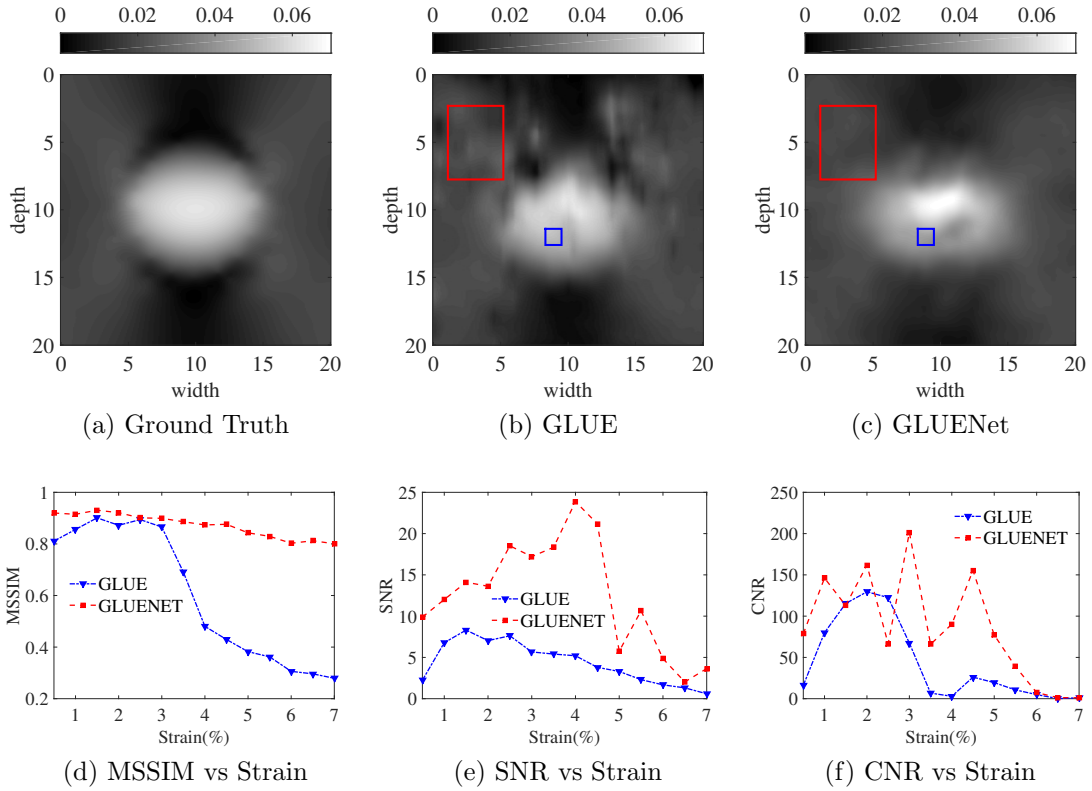

Figure 5: First row shows axial strain images of simulation phantom with added random noise (PSNR: 12.7 dB); (a) Ground truth, (b) GLUE and (c) GLUENet. Second row shows the performance metrics graph with respect to various range of applied strain; (d) MSSIM vs Strain, (e) SNR vs Strain and (f) CNR vs Strain.

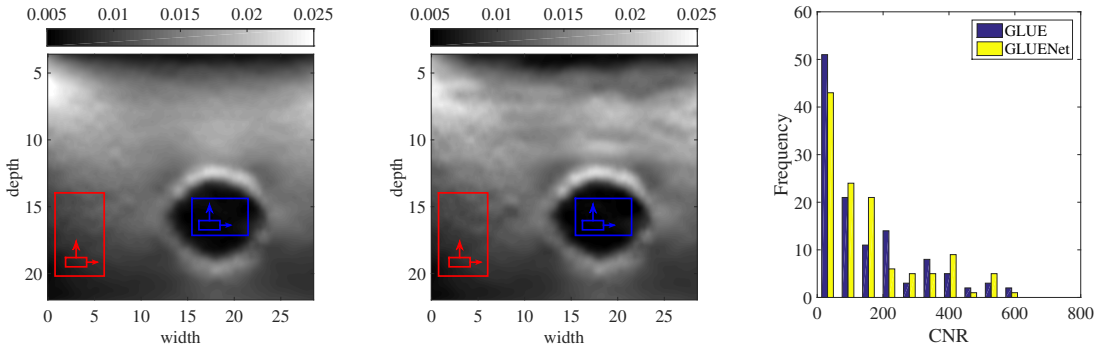

Figure 6: Axial strain images of experimental phantom data generated by (a) GLUE and (b) GLUENet, and (c) histogram of CNR values of GLUE and GLUENet.

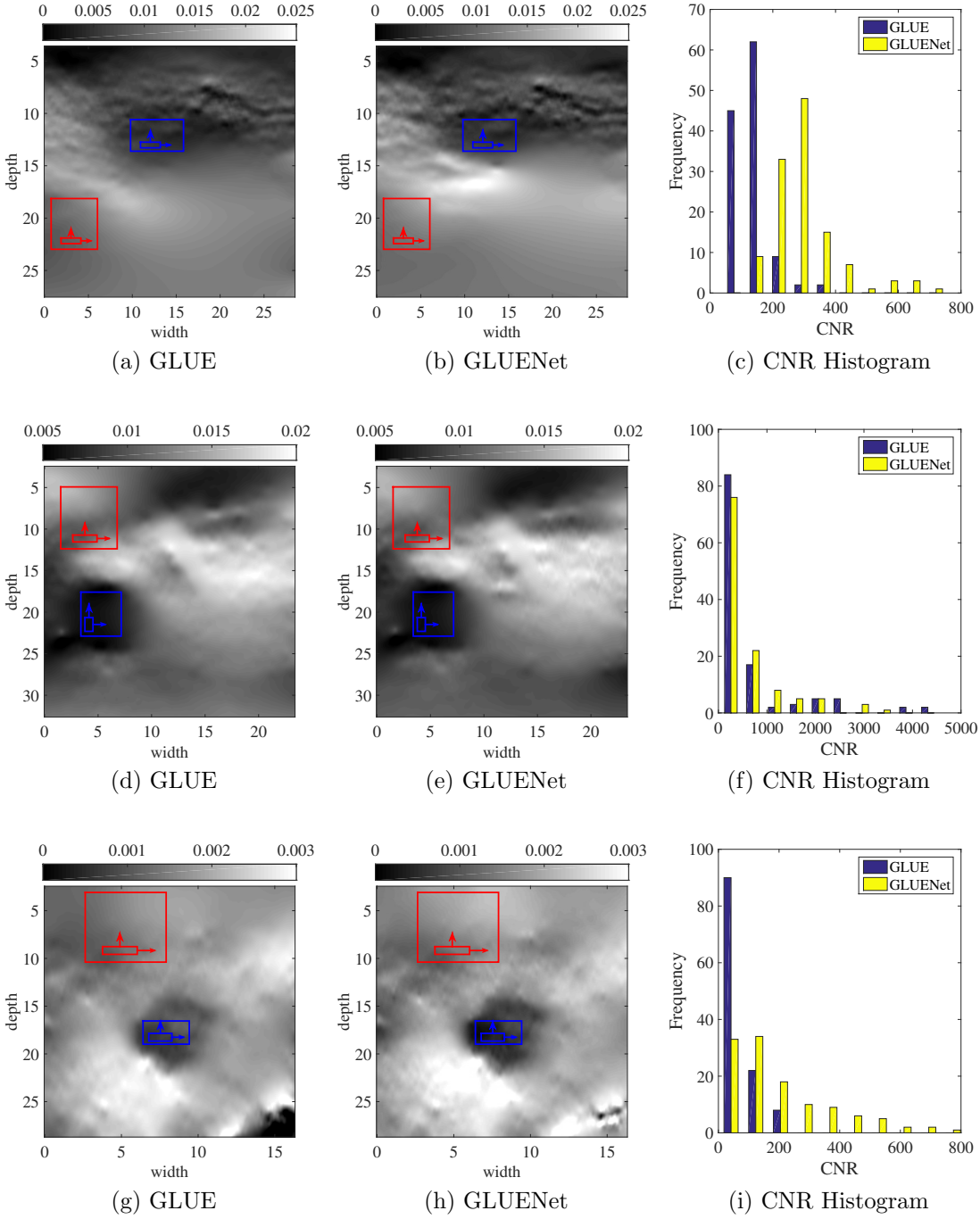

(a) GLUE (b) GLUENet (c) CNR Histogram

(d) GLUE (e) GLUENet (f) CNR Histogram

(g) GLUE (h) GLUENet (i) CNR Histogram

Figure 7: Axial strain images of patients and histogram of CNR values: The three rows correspond to patients 1-3 respectively. First and second columns depict axial strain images from GLUE and GLUENet respectively. Third column shows histogram of CNR values of GLUE and GLUENet.

high frequency at high CNR values while GLUE is more frequent at low values. Table 1 shows the SNR and CNR values for all patients which is calculated by using the large blue and red windows as target and background. We calculate failure rate of GLUE and GLUENet from 392 pre- and post- compression RF echo frame pairs chosen from 60 RF echo frames of all three patients. The best axial strain is marked visually to compare with other strains using NCC. A threshold of 0.6 is used to determine the failure rate of the methods shown in Table 1. The failure rate of GLUENet is very low compared to GLUE for all patient data thus proving the robustness of GLUENet to decorrelation noise in clinical data.

2.4 Discussion

The failure rates of GLUE in Table 1 are generally high because no parameter tuning is performed for the hyperparameters. Another reason for high failure rates is that we select pairs of frames that are temporally far from each other to test the robustness at extreme levels. This substantially increases non-axial motion of the probe and complex biological motions, which leads to severe decorrelation in the RF signal. In real-life, the failure rate of these methods can be improved by selecting pairs of RF data that are not temporally far from each other. In this experiment, no external outliers is introduced for testing robustness. If introduced, the failure rate for both GLUE and GLUENet would have been increased.

2.5 Summary

In this chapter, we introduced a novel technique to calculate tissue displacement from ultrasound images using CNN. This is, to the best of our knowledge, the first use of CNN for estimation of displacement in ultrasound elastography. The

displacement estimation obtained from CNN was further refined using GLUE [63], and therefore, we referred to our method as GLUENet. We showed that GLUENet is robust to decorrelation noise in simulation, experiments and *in-vivo* data, which makes it a good candidate for clinical use. In addition, the high robustness to noise allows elastography to be performed by less experienced sonographers as a point-of-care imaging tool.

Chapter 3

A Transfer Learning Approach for using Convolutional Neural Network in Ultrasound Elastography

Ultrasound elastography is a cost-effective, portable medical imaging modality which can provide significant diagnostic information about a biological tissue in real-time by imaging its elastic properties. Displacement estimation is the most critical step in ultrasound elastography as it suffers from various sources of noise such as decorrelation noise, jitter noise etc. and can severely compromise the quality of the calculated strain image. CNNs can be effectively used for addressing the noise effects in displacement estimation as the ultrasound data is filtered and processed in local and global perspective while being forwarded through the convolutional neural network architecture. In this chapter, we propose fine-tuning the weights of a recently reported network trained for optical flow estimation. The multi-level deep architecture of convolutional neural network helps the process of

displacement estimation become more robust to the decorrelation noise. We test our theory using simulation and experimental phantom data.

3.1 Introduction

While some ultrasound elastography algorithms [31, 48, 49] calculate strain image directly from the pre- and post-compression ultrasound RF frames, most of them [5,6,25,62,63] estimate displacement field and then calculate strain image by spatial differentiation of the displacement map using least-square or gradient methods. Consequently, displacement estimation is a critical step in ultrasound elastography and it faces crucial challenges from different sources of noise such as decorrelation noise, jitter noise etc. Decorrelation noise can severely affect the displacement estimation which in turn can affect the quality of the estimated strain image. Conventional ultrasound elastography algorithms use cross-matching techniques such cross-correlation, similarity, sum of difference etc. on selected overlapping windows or pixels to track the displacement between two corresponding ultrasound RF frames. These methods are more susceptible to decorrelation noise due to the fact that they consider a small portion of the whole ultrasound RF frame for displacement estimation. This makes the depth of field, the effective area of the RF frame, for calculating displacement very shallow. Including the neighbourhood pixel/window information can help broaden the depth of field thus improving the robustness of displacement estimation.

Advanced machine learning techniques such as CNNs can provide a wide depth of field on different layers and levels. This kind of deep network architecture should provide more robustness in displacement estimation, at least theoretically, as different patch-sized data of ultrasound RF frame is used at different levels of the network compared to the fixed-length window-based or pixel-based methods.

The fact that machine learning techniques like CNN can be trained on a data set designed for a specific task makes it more powerful for filtering out unwanted noise and artifacts. Another unique characteristic of CNN is that previously trained and optimized network can be fine-tuned on a new and similar training data set designed for a task related to the one it was originally trained for. This exhibits the powerful feature CNNs have wherein they can transfer the knowledge it gained from previous training to the next step. This is widely known as transfer learning which makes it possible to skip the unnecessary and tedious job of designing and training a CNN from scratch. Rather the smart move here is to build on what have been achieved so far. This has become the normal practice in CNN through the process of transfer learning.

The process of transfer learning works effectively, when there exists a network already trained for an analogous task. As it happens, the task of displacement estimation in ultrasound elastography is analogous to the task of optical flow estimation in computer vision in the sense that in both cases motion of pixels is tracked between two images directly correlated by a displacement field. Recently, CNN architectures [71,75] heavily trained and optimized for optical flow estimation have shown promising result in terms of quality of the flow estimation and real-time performance which can be used for displacement estimation in ultrasound elastography using transfer learning.

In this chapter, we investigate the impact of transfer learning in displacement estimation for ultrasound elastography. In Section 3.2, we discuss possible ways of transfer learning, involved data sets and training schedules. In Section 3.3, we test the performance of our fine-tuned network using simulation and experimental phantom, and clinical data. We discuss our observation on the training procedure and the results in Section 3.4.

3.2 Method

We retrain FlowNet 2.0 architecture with slight adjustment to the network for fine-tuning its weights for the purpose of improving the displacement estimation from ultrasound images. We use simulated ultrasound images for the fine-tuning.

3.2.1 FlowNet 2.0 architecture

The building blocks of FlowNet 2.0 architecture contain FlowNetS and FlowNetC architectures. FlowNetC and FlowNetS were originally proposed by Dosovitskiy *et al.* [75]. FlowNetS is a generic U-Net architecture trained for optical flow estimation. U-Net architecture is best known for the task of semantic segmentation and per-pixel prediction making it an excellent choice for optical flow estimation and displacement estimation. The U-Net architecture maintains a encoder-decoder form where the input image is encoded by the encoder part of the network and useful features are extracted from the input. The decoder part of the network decodes the encoded features to the desired semantic presentation such as displacement estimation. FlowNetC is a variation of FlowNetS which includes a non-trainable cross-correlation layer. Cross-correlation is a popular block-matching technique in flow estimation and understandably FlowNetC gets a boost in performance compared to FlowNetS [71]. The biggest breakthrough of FlowNet architectures were the real-time execution of optical flow estimation while achieving almost same performance as the state-of-the-art methods.

FlowNet 2.0 improves its performance in optical flow estimation by stacking FlowNetC and FlowNetS on top of each other and adhrering to a specific training schedule. The quality of the optical flow estimation was as good as the state-of-the art methods while performing in real-time. Figure 4 represents the final FlowNet 2.0 architecture. The pipeline of one FlowNetC and two FlowNetS networks

were trained with datasets which includes mostly large displacements. Another FlowNetS network was trained with datasets having small displacements for more fine estimation of small displacements. The output of these two pipeline of networks are fused together with a small Fusion network, which also is a generic U-Net architecture, to yield the final flow estimation.

3.2.2 Training Dataset

FlowNet 2.0 network was trained with a dataset which contains more than 22000 training samples. Each training sample contains an image pairs and their corresponding ground truth optical flow. The whole dataset was synthetically designed by placing chairs on different randomly selected background. The chairs were moved with respect to the background to make the corresponding image pair and ground truth optical flow. The number of training samples in the dataset seems large enough to train FlowNet 2.0 to achieve nearly state-of-the-art performance. For fine-tuning FlowNet 2.0 for estimating displacement from ultrasound images, we used a dataset of simulated ultrasound images of 2000 training samples. The only way to get ground truth displacement from corresponding ultrasound images is to simulate the ultrasound images. Each training sample contains two ultrasound images with ground truth axial and lateral displacement. The simulation phantoms in the dataset contains inclusions of various numbers, sizes and positions. The axial and lateral displacements of the simulation phantoms, subjected to various degrees of external pressure resulting in various degrees of applied strain, was calculated using Finite Element Method from Abaqus and Ansys. This displacement map is our ground truth for training purpose. The ultrasound image is simulated using Field II [80] software. The center frequency of ultrasound was set to 5 MHz and the sampling rate of the probe was set to 40 MHz. The simulation phantom data we used for comparing the improvement in displacement estimation

is completely different set from the ones we used for fine-tuning the FlowNet 2.0 model. This phantom contains a single lesion which is softer than its surrounding tissue. The ultrasound RF data was simulated at 5MHz with a sample rate of 40 MHz. Complete details of the simulation phantom can be found here [5]

3.2.3 Fine-tuning FlowNet 2.0

FlowNet 2.0 is a very large convolutional network as a whole with stacks of sub-networks on top of each other. FlowNet 2.0 weights have been obtained by following a specific training schedule and datasets. Details of the training schedules and datasets can be found here [71]. The input to the network is a pair of images which are correlated by a flow or motion of one or more objects in the images. The ground truth contains the flow of the any object present in the pair of images in both horizontal and vertical direction. The task of the network is to predict the flow as close as to the ground truth given two images having flow information.
At first, we fine-tune FlowNetS with ultrasound images. The calculated displacement estimation is not good enough to extract any meaningful displacement or strain information. Then we fine-tune FlowNetC yielding no notable improvement. FlowNet 2.0 is originally trained following a very complex and sophisticated schedule. Fine-tuning FlowNet 2.0 according to the original steps and schedule is very challenging. Finally we fine-tune the entire FlowNet 2.0 network with ultrasound images. Tissues without tumor/inclusion such as homogenous tissue, tissues with different layers etc. can be introduced during first stages of fine-tuning, gradually exposing the network to more complex datasets.

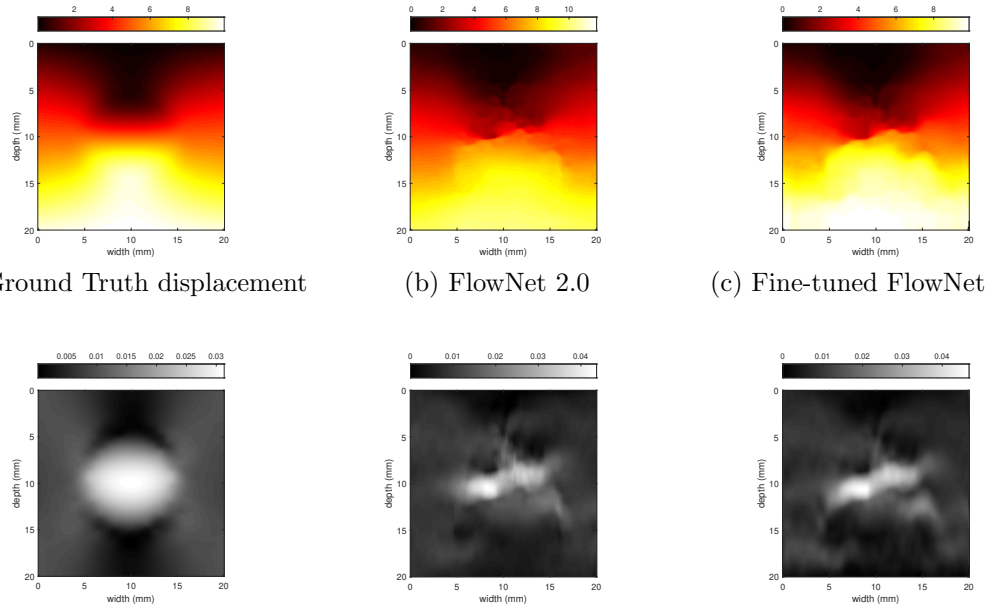

(a) Ground Truth displacement (b) FlowNet 2.0 (c) Fine-tuned FlowNet 2.0

(d) Ground Truth Strain (e) FlowNet 2.0 (f) Fine-tuned FlowNet 2.0

Figure 8: First row shows displacement estimation of simulation phantom; (a) Ground truth, (b) FlowNet 2.0 and (c) Fine-tuned FlowNet 2.0. Second row shows the axial strain images of simulation phantom ; (d) Ground truth, (e) FlowNet 2.0 and (f) Fine-tuned FlowNet 2.0.

3.3 Results

In this chapter, the goal was to improve the quality of displacement estimation by FlowNet 2.0 to a degree that it is possible to extract strain image from the displacement estimation without the necessity of refinement of dispalcement estimation through GLUE. We tested the efficacy of fine-tuned weights of the model by comparing displacement estimation and strain estimation using gradient based or least-square based methods. We use computed simutated phantom and experimental phantom data for such purpose.

3.3.1 Simulation Phantom

Figure 8 shows the results in simulation phantom. The first row corresponds to the estimated displacement fields by the networks. Second row corresponds

to strain estimation from the displacement using least-square or gradient-based methods. The columns correspond to the results obtained from FlowNet 2.0 and the fine-tuned FlowNet 2.0 respectively. The improvement of the displacement estimation for fine-tuning the network is clearly not enough for strain estimation using least-square or gradient-based method. The overall strain estimation is smoother by fine-tuned network as a result of a subtle improvement in displacement estimation.

3.3.2 Experimental Phantom

Our experimental phantom is a CIRS tissue mimicking phantom. We used ultrasound machine to take RF data from the CIRS phantom. The Region Of Interest (ROI) of the ultrasound scan contains a hard inculsion compared to the surrounding softer tissue. Figure 9 shows the results obtained using experimental phantoms. The first row shows the estimated displacement and the second row shows strain images obtained from the displacement using least-square or gradient-based method. The first column corresponds to the results obtained from FlowNet 2.0 network and the second column correspond to the results obtained from fine-tuning FlowNet 2.0 network. The improvement in displacement estimation for fine-tuning the network is evident in the smoothness of the strain estimation by fine-tuned FlowNet 2.0. Although the improved result is not upto the level of the state-of-the-art elastography algorithm, this slight improvement indicates that the displacement can be improved to a much satisfactory level with proper scheduling of training and proper amount of training data.

3.4 Discussion

In this chapter, our goal was to retrain FlowNet 2.0 with ultrasound elastography dataset to improve displacement estimation between two corresponding ultrasound images to a satisfactory level where fine-tuning the estimated displacement from FlowNet 2.0 deems unnecessary for quality strain image. After some modification of the FlowNet 2.0 architecture and retraining, the subtle improvement acheived is not good enough for generating strain images competetive with the quality of the state-of-the-art elastography images. But the small improvement suggests the possibility of more meaningful improvement in displacement estimation for ultrasound elastography. From the results we can observe that the fine-tuned network has achieved finer and smoother displacement than achieved from FlowNet 2.0 network. It is also noticeable that the lesion/inclusion structure integrity is not depicted in the strain images derived from the displacement estimation in both FlowNet 2.0 and its fine-tuned version. It may be for the reason that the FlowNet 2.0 network was originally trained with a dataset where the objects have displacements while the background remained stationary. This may be okay for general optical flow estimation but the displacement profile in ultrasound elastography is somewhat different and has a physical restriction. As it happens, biological tissues are physically attached to one another on different layers and any displacement introduced during ultrasound elastography is tightly coupled, that is, the background and the lesion both have different level of displacement depending upon their strain profile. This fact introduces the restriction that the displacement estimated in one region of interest along a scan line should be similar to the neighboring regions of interest. In other words, displacement should not have a sharp change rather a gradual change at different level of strain. This is an important regularization feature considered in almost every conventional

elastography algorithms. The dataset used in training FlowNet 2.0 lacks this property which may be the reason FlowNet 2.0 has difficulty in retaining the shape and edge of the lesion in strain images. Another way to improve the performance is to incorporate more correlated data in the network. At least two ultrasound images are required for displacement estimation but more correlated ultrasound images in temporal domain have shown better results in displacement estimation [6].

The most suitable organs for ultrasound elastography are breast tissue, liver, prostate etc. As ultrasound cannot penetrate bones ultrasound elastography of the organs protected by bones such as heart, brain, lungs etc. are more challenging. Although ultrasound is inexpensive but it requires extensive training of a sonographer for obtaining diagnostically meaningful images from ultrasound. This is more true for ultrasound elastography. Hopefully introduction of machine learning techniques would acheive such improved system that highly expertise from human would not be needed anymore. But for that more rigorous testing with much more data from various sources and parts of the body is required for evaluating the fine-tuning results for any future clinical application approvals.

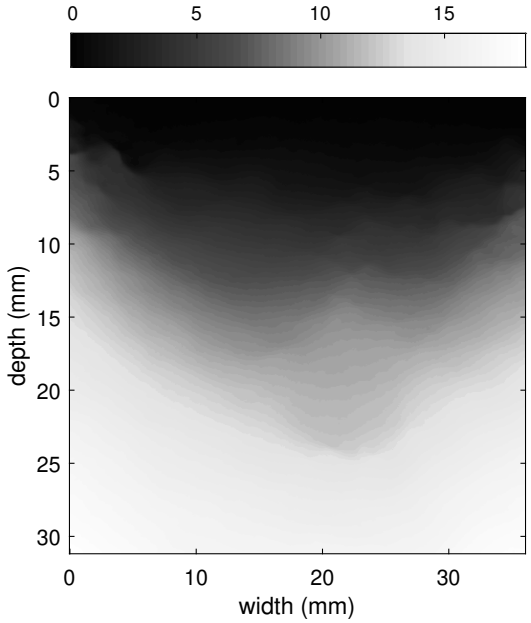

(a) Displacement from FlowNet 2.0

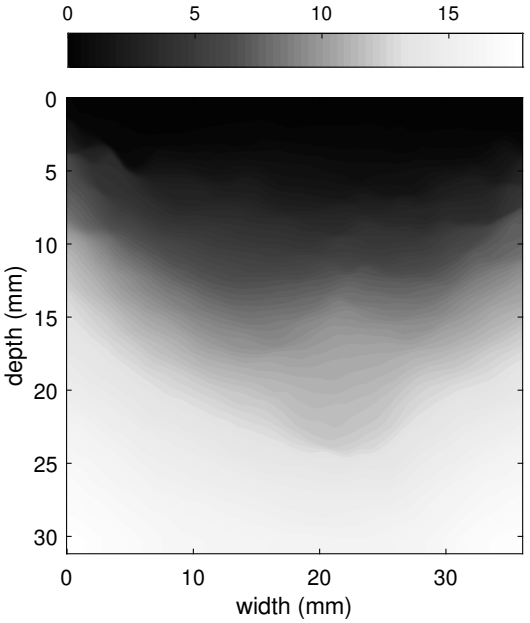

(b) Displacement from Fine-tuned FlowNet 2.0

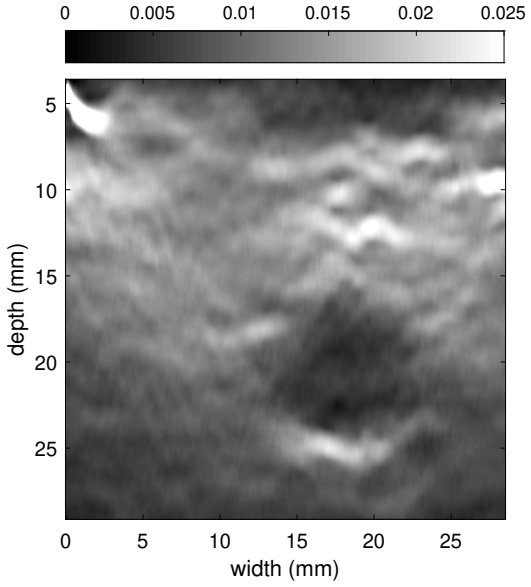

(c) Strain from FlowNet 2.0

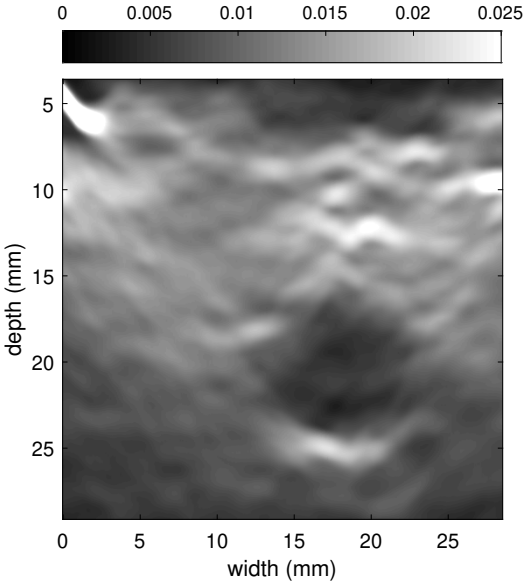

(d) Strain from Fine-tuned FlowNet 2.0

Figure 9: First row shows displacement estimation of experimental phantom; (a) FlowNet 2.0 and (b) Fine-tuned FlowNet 2.0. Second row shows the strain image of experimental phantom; (a) FlowNet 2.0 and (b) Fine-tuned FlowNet 2.0.

Chapter 4

Discussion and Future Work

4.1 Concluding Remark

In this chapter we discuss our findings and propose avenues for future work. In this thesis our goal was to use the convolutional neural network architecture for displacement estimation in ultrasound elastography. In Chapter 2 FlowNet 2.0 architecture was used for displacement estimation from two corresponding ultrasound images. The estimated displacement is robust to decorrelation noise but was not fine enough to extract strain images of the quality of those of state-of-the-art ultrasound elastography algorithms. The coarse displacement estimation was further fine-tuned by a global optimization based algorithm GLUE which uses coarse initial displacement estimate for calculating finer displacement estimation. We call our method GLUENet which collectively produces fine displacement estimation and quality strain images while being robust to decorrelation noise.

In Chapter 3, our goal was to use transfer learning technique to fine-tune the already trained weights of FlowNet 2.0 architecture so that finer displacement estimation can be achieved for quality strain images. FlowNet 2.0 was trained

with specific datasets and complex training schedules for optical flow estimation. Although optical flow estimation is very similar to ultrasound displacement estimation, the characteristics of input data has a fundamental difference. The target dataset for optical flow estimation mostly includes RGB pictures or movie frames with one or more object freely moving with respect to its background where the spatial frequency in both axial and lateral direction is the same. Ultrasound data is normally a collection of axial scans from an array of ultrasound transducers where spatial frequency in the axial direction is higher compared to the spatial frequency in lateral direction. The difficulties in retraining the weights of FlowNet 2.0 were two-folds. Firstly, the architecture of the whole network involved multi-level stacking and hence the training schedule was complicated. Secondly, the volume of the original training dataset for FlowNet 2.0 was very large whereas the available simulation dataset of ultrasound elastography for training was very small in comparison due to computation complexity of the simulation. When fine-tuning with such small amount of training data, there is a tendency of overfitting which distorts the displacement estimation. As a result, the outcome loses its semantic value and the size, position, shape and contrast of the lesion is not recognizable beyond doubt from the strain images. The best result obtained in Chapter 3 shows that the estimated displacement gets smoother as a result of fine-tuning FlowNet 2.0. Therefore, more studies are needed to improve the results, as outlined in the following section.

4.2 Future Work

CNN has opened a new domain of works in ultrasound elastography. This deep learning technique provides robustness to common sources of noises in ultrasound elastography while generating useful displacement information. In this thesis,

FlowNet 2.0 was chosen as the target CNN architecture for ultrasound elastography because it has reported the best results in optical flow estimation to the best of our knowledge. There are many possibilities where we can extend our work in the following technical avenues.

- The output of FlowNet 2.0 for optical flow estimation and ultrasound elastography is almost identical in the sense that in both cases displacement estimation is extracted from two corresponding images. The inputs for optical flow estimation and ultrasound elastography differs in the sense of nature of the data. Therefore, it is intuitional and logical that the first few layers of each stack of FlowNet 2.0 architecture should be fine-tuned rather than fine-tuning the last couple of layers which is common practice in transfer learning. New layers can be introduced and retrained with ultrasound data at the beginning of the network so that useful features can be extracted from ultrasound data and passed to the following layers for better displacement estimation. A recent work from our group studied how selection of layers for fine-tuning can affect the results [82], and it is interesting to apply this framework to ultrasound elastography.

- In Chapter 2 the coarse displacement estimation from FlowNet 2.0 was further refined by GLUE. A U-Net architecture can be used and trained to obtain this refinement. This trained architecture can be stacked following FlowNet 2.0 architecture. This approach will make a complete end to end architecture and possibly be more robust and faster.

- The FlowNet 2.0 architecture while producing state-of-the-art quality optical flow estimation involves complex structure which makes the training schedule more complex. A single U-Net architecture can be used and trained from scratch for ultrasound elastography.

The deep learning methods specially CNNs have shown excellent performance in semantic augmentation. Moreover the concept of transfer learning has introduced endless possibilities specially in medical imaging. The nature of ultrasound elastography algorithms are best suited for CNNs specially those architectures aimed for semantic augmentation and per-pixel prediction. A successful endeavor in one area of ultrasound imaging can be carried forward to different related areas through transfer learning. In this thesis, we have successfully utilized the convolutional neural network techniques for ultrasound elastography. We also ventured in transfer learning to improve the performance of the network. While the introduction of ultrasound imaging in deep learning domain has been a success, transfer learning proved to be more challenging and need more work for achieving performance to match that of traditional techniques.

Bibliography

[1] Jonathan Ophir, S Kaisar Alam, Brian Garra, F Kallel, E Konofagou, T Krouskop, and T Varghese. Elastography: ultrasonic estimation and imaging of the elastic properties of tissues. *Proceedings of the Institution of Mechanical Engineers, Part H: Journal of Engineering in Medicine*, 213(3):203–233, 1999.

[2] Katharina König, Ulrich Scheipers, Andreas Pesavento, Andreas Lorenz, Helmut Ermert, and Theodor Senge. Initial experiences with real-time elastography guided biopsies of the prostate. *J. Urol.*, 174(1):115–117, 2005.

[3] Masakazu Tsutsumi, Tomoaki Miyagawa, Takeshi Matsumura, Natsui Kawazoe, Satoru Ishikawa, Tatsuro Shimokama, Tsuyoshi Shiina, Naoto Miyanaga, and Hideyuki Akaza. The impact of real-time tissue elasticity imaging (elastography) on the detection of prostate cancer: clinicopathological analysis. *Int. J. Clin. Oncol.*, 12(4):250–255, 2007.

[4] Mireen Friedrich-Rust, Mei-Fang Ong, Eva Herrmann, Volker Dries, Panagiotis Samaras, Stefan Zeuzem, and Christoph Sarrazin. Real-time elastography for noninvasive assessment of liver fibrosis in chronic viral hepatitis. *Am. J. Roentgenol.*, 188(3):758–764, 2007.

[5] Hassan Rivaz, Emad M Boctor, Michael A Choti, and Gregory D Hager. Real-time regularized ultrasound elastography. *IEEE Trans. Med. Imaging*, 30(4):928–945, 2011.

[6] M. Ashikuzzaman, C. J. Gauthier, and H. Rivaz. Global ultrasound elastography in spatial and temporal domains. *IEEE Transactions on Ultrasonics, Ferroelectrics, and Frequency Control*, 66(5):876–887, May 2019.

[7] An Tang, Guy Cloutier, Nikolaus M Szeverenyi, and Claude B Sirlin. Ultrasound elastography and mr elastography for assessing liver fibrosis: part 2, diagnostic performance, confounders, and future directions. *American journal of roentgenology*, 205(1):33–40, 2015.

[8] Tomy Varghese, JA Zagzebski, and FT Lee Jr. Elastographic imaging of thermal lesions in the liver in vivo following radiofrequency ablation: preliminary results. *Ultrasound in medicine & biology*, 28(11-12):1467–1473, 2002.

[9] Tomy Varghese, Udomchai Techavipoo, Wu Liu, James A Zagzebski, Quan Chen, Gary Frank, and Fred T Lee Jr. Elastographic measurement of the area and volume of thermal lesions resulting from radiofrequency ablation: pathologic correlation. *American journal of roentgenology*, 181(3):701–707, 2003.

[10] Hassan Rivaz, Ioana Fleming, Lia Assumpcao, Gabor Fichtinger, Ulrike Hamper, Michael Choti, Gregory Hager, and Emad Boctor. Ablation monitoring with elastography: 2d in-vivo and 3d ex-vivo studies. In *International Conference on Medical Image Computing and Computer-Assisted Intervention*, pages 458–466. Springer, 2008.

[11] A Mariani, W Kwiecinski, M Pernot, D Balvay, M Tanter, O Clement, CA Cuenod, and F Zinzindohoue. Real time shear waves elastography monitoring of thermal ablation: in vivo evaluation in pig livers. *Journal of Surgical Research*, 188(1):37–43, 2014.

[12] Christian Vorländer, Jan Wolff, Said Saalabian, Robert H Lienenlüke, and Robert A Wahl. Real-time ultrasound elastography—a noninvasive diagnostic procedure for evaluating dominant thyroid nodules. *Langenbeck's Arch. Surg.*, 395(7):865–871, 2010.

[13] Anke Thomas, Friedrich Degenhardt, André Farrokh, Sebastian Wojcinski, Torsten Slowinski, and Thomas Fischer. Significant differentiation of focal breast lesions: calculation of strain ratio in breast sonoelastography. *Acad. Radiol.*, 17(5):558–563, 2010.

[14] Brian S Garra, E Ignacio Cespedes, J Ophir, Stephen R Spratt, Rebecca A Zuurbier, Colette M Magnant, and Marie F Pennanen. Elastography of breast lesions: initial clinical results. *Radiology*, 202(1):79–86, 1997.

[15] Timothy J Hall, Yanning Zhu, and Candace S Spalding. In vivo real-time freehand palpation imaging. *Ultrasound in Medicine and Biology*, 29(3):427–435, 2003.

[16] Adib Nahiyan and Md Kamrul Hasan. Hybrid algorithm for elastography to visualize both solid and fluid-filled lesions. *Ultrasound in medicine & biology*, 41(4):1058–1078, 2015.

[17] Jingfeng Jiang and Timothy J Hall. A coupled subsample displacement estimation method for ultrasound-based strain elastography. *Physics in Medicine & Biology*, 60(21):8347, 2015.

[18] Hoda S Hashemi, Stefanie Fallone, Mathieu Boily, Anna Towers, Robert D Kilgour, and Hassan Rivaz. Assessment of mechanical properties of tissue in breast cancer-related lymphedema using ultrasound elastography. *IEEE transactions on ultrasonics, ferroelectrics, and frequency control*, 66(3):541–550, 2018.

[19] Sharmin R Ara, Syed Khairul Bashar, Farzana Alam, and Md Kamrul Hasan. Emd-dwt based transform domain feature reduction approach for quantitative multi-class classification of breast lesions. *Ultrasonics*, 80:22–33, 2017.

[20] Thomas Gallot, Stefan Catheline, Philippe Roux, Javier Brum, Nicolas Benech, and Carlos Negreira. Passive elastography: shear-wave tomography from physiological-noise correlation in soft tissues. *IEEE transactions on ultrasonics, ferroelectrics, and frequency control*, 58(6):1122–1126, 2011.

[21] Ivan M Rosado-Mendez, Lindsey C Carlson, Kaitlin M Woo, Andrew P Santoso, Quinton W Guerrero, Mark L Palmeri, Helen Feltovich, and Timothy J Hall. Quantitative assessment of cervical softening during pregnancy in the rhesus macaque with shear wave elasticity imaging. *Physics in Medicine & Biology*, 63(8):085016, 2018.

[22] Mahmoud Derakhshan Horeh, Amir Asif, and Hassan Rivaz. Analytical minimization-based regularized subpixel shear-wave tracking for ultrasound elastography. *IEEE transactions on ultrasonics, ferroelectrics, and frequency control*, 66(2):285–296, 2018.

[23] Kathryn Nightingale, Mary Scott Soo, Roger Nightingale, and Gregg Trahey. Acoustic radiation force impulse imaging: in vivo demonstration of clinical feasibility. *Ultrasound in medicine & biology*, 28(2):227–235, 2002.

[24] Jonathan Ophir, Ignacio Cespedes, Hm Ponnekanti, Youseph Yazdi, and Xin Li. Elastography: a quantitative method for imaging the elasticity of biological tissues. *Ultrasonic imaging*, 13(2):111–134, 1991.

[25] Md Golam Kibria and Md Kamrul Hasan. A class of kernel based real-time elastography algorithms. *Ultrasonics*, 61:88–102, 2015.

[26] Xiaochang Pan, Ke Liu, Jinghua Shao, Jing Gao, Lingyun Huang, Jing Bai, and Jianwen Luo. Performance comparison of rigid and affine models for motion estimation using ultrasound radio-frequency signals. *IEEE transactions on ultrasonics, ferroelectrics, and frequency control*, 62(11):1928–1943, 2015.

[27] Jiaqi Wang, Qinghua Huang, and Xin Zhang. Ultrasound elastography based on the normalized cross-correlation and the pso algorithm. In *2017 4th International Conference on Systems and Informatics (ICSAI)*, pages 1131–1135. IEEE, 2017.

[28] Lili Yuan and Peder C Pedersen. Analytical phase-tracking-based strain estimation for ultrasound elasticity. *IEEE transactions on ultrasonics, ferroelectrics, and frequency control*, 62(1):185–207, 2015.

[29] Reza Zahiri-Azar and Septimiu E Salcudean. Motion estimation in ultrasound images using time domain cross correlation. *IEEE TMB*, 53(10):1990–2000, 2006.

[30] Andrey Kuzmin, Aaron M Zakrzewski, Brian W Anthony, and Victor Lempitsky. Multi-frame elastography using a handheld force-controlled ultrasound probe. *IEEE transactions on ultrasonics, ferroelectrics, and frequency control*, 62(8):1486–1500, 2015.

[31] Sharmin R. Ara, Faisal Mohsin, Farzana Alam, S. A. Rupa, Soo Yeol Lee, M. K. Hasan, and R. Awwal. Phase-based direct average strain estimation for elastography. *IEEE Trans. Ultrason. Ferroelectr. Freq. Control*, 60(11):2266–2283, 2013.

[32] Faouzi Kallel and Jonathan Ophir. A least-squares strain estimator for elastography. *Ultrason. Imaging*, 19(3):195–208, 1997.

[33] RJ Dickinson and CR Hill. Measurement of soft tissue motion using correlation between a-scans. *Ultrasound in medicine & biology*, 8(3):263–271, 1982.

[34] Emad S Ebbini. Phase-coupled two-dimensional speckle tracking algorithm. *IEEE transactions on ultrasonics, ferroelectrics, and frequency control*, 53(5):972–990, 2006.

[35] Graham M Treece, Joel E Lindop, Andrew H Gee, and Richard W Prager. Freehand ultrasound elastography with a 3-d probe. *Ultrasound in medicine & biology*, 34(3):463–474, 2008.

[36] Morteza Mirzaei, Amir Asif, Maryse Fortin, and Hassan Rivaz. 3d normalized cross-correlation for estimation of the displacement field in ultrasound elastography. *Ultrasonics*, 102:106053, 2020.

[37] Jianwen Luo and Elisa E Konofagou. Effects of various parameters on lateral displacement estimation in ultrasound elastography. *Ultrasound in medicine & biology*, 35(8):1352–1366, 2009.

[38] Qiong He, Ling Tong, Lingyun Huang, Jing Liu, Yinran Chen, and Jianwen Luo. Performance optimization of lateral displacement estimation with spatial angular compounding. *Ultrasonics*, 73:9–21, 2017.

[39] S Kaisar Alam, Jonathan Ophir, and Elisa E Konofagou. An adaptive strain estimator for elastography. *IEEE Trans. Ultrason. Ferroelectr. Freq. Control*, 45(2):461–472, 1998.

[40] T Varghese, EE Konofagou, J Ophir, SK Alam, and M Bilgen. Direct strain estimation in elastography using spectral cross-correlation. *Ultrasound Med. Biol.*, 26(9):1525–1537, 2000.

[41] S Kaisar Alam, Frederic L Lizzi, Tomy Varghese, Ernest J Feleppa, and Sarayu Ramachandran. Adaptive spectral strain estimators for elastography. *Ultrason. imaging*, 26(3):131–149, 2004.

[42] Joel E Lindop, Graham M Treece, Andrew H Gee, and Richard W Prager. Estimation of displacement location for enhanced strain imaging. *IEEE Trans. Ultrason. Ferroelectr. Freq. Control*, 54(9):1751–1771, 2007.

[43] Andreas Pesavento, Christian Perrey, Martin Krueger, and Helmut Ermert. A time-efficient and accurate strain estimation concept for ultrasonic elastography using iterative phase zero estimation. *IEEE TUFFC*, 46(5):1057–1067, 1999.

[44] A Pesavento and H Ermert. Time-efficient and exact algorithms for adaptive temporal stretching and 2D-correlation for elastographic imaging using phase information. In *IEEE Int. Ultrason. Symp.*, volume 2, pages 1765–1768. IEEE, 1998.

[45] Tsuyoshi Shiina, Naotaka Nitta, EI Ueno, and Jeffrey C Bamber. Real time tissue elasticity imaging using the combined autocorrelation method. *Journal of Medical Ultrasonics*, 29(3):119–128, 2002.

[46] Joel E Lindop, Graham M Treece, Andrew H Gee, and Richard W Prager. Phase-based ultrasonic deformation estimation. *IEEE Trans. Ultrason. Ferroelectr. Freq. Control*, 55(1):94–111, 2008.

[47] Elisabeth Brusseau, Jérémie Fromageau, Gérard Finet, Philippe Delachartre, and Didier Vray. Axial strain imaging of intravascular data: results on polyvinyl alcohol cryogel phantoms and carotid artery. *Ultrasound Med. Biol.*, 27(12):1631–1642, 2001.

[48] Mohammad Arafat Hussain, Emran Mohammad Abu Anas, S Kaisar Alam, Soo Yeol Lee, and Md Kamrul Hasan. Direct and gradient-based average strain estimation by using weighted nearest neighbor cross-correlation peaks. *IEEE TUFFC*, 59(8):1713–1728, 2012.

[49] Md Kamrul Hasan, Emran Mohammad Abu Anas, S Kaisar Alam, and Soo Yeol Lee. Direct mean strain estimation for elastography using nearest-neighbor weighted least-squares approach in the frequency domain. *Ultrasound Med. Biol.*, 38(10):1759–1777, 2012.

[50] Rashid Al Mukaddim, Nirvedh H Meshram, and Tomy Varghese. Locally optimized correlation-guided bayesian adaptive regularization for ultrasound strain imaging. *Physics in Medicine & Biology*, 65(6):065008, 2020.

[51] Matthew McCormick, Nicholas Rubert, and Tomy Varghese. Bayesian regularization applied to ultrasound strain imaging. *IEEE transactions on biomedical engineering*, 58(6):1612–1620, 2011.

[52] Brett Byram, Gregg E Trahey, and Mark Palmeri. Bayesian speckle tracking. part ii: biased ultrasound displacement estimation. *IEEE transactions on ultrasonics, ferroelectrics, and frequency control*, 60(1):144–157, 2012.

[53] Douglas M Dumont, Kristy M Walsh, and Brett C Byram. Improving displacement signal-to-noise ratio for low-signal radiation force elasticity imaging using bayesian techniques. *Ultrasound in medicine & biology*, 42(8):1986–1997, 2016.

[54] Udomchai Techavipoo, Quan Chen, Tomy Varghese, and James A Zagzebski. Estimation of displacement vectors and strain tensors in elastography using angular insonifications. *IEEE transactions on medical imaging*, 23(12):1479–1489, 2004.

[55] Ted G Fisher, Timothy J Hall, Satchi Panda, Michael S Richards, Paul E Barbone, Jingfeng Jiang, Jeff Resnick, and Steve Barnes. Volumetric elasticity imaging with a 2-d cmut array. *Ultrasound in medicine & biology*, 36(6):978–990, 2010.

[56] Yuqi Wang, Jingfeng Jiang, and Timothy J Hall. A 3-d region-growing motion-tracking method for ultrasound elasticity imaging. *Ultrasound in medicine & biology*, 44(8):1638–1653, 2018.

[57] Clement Papadacci, Ethan A Bunting, Elaine Y Wan, Pierre Nauleau, and Elisa E Konofagou. 3d myocardial elastography in vivo. *IEEE transactions on medical imaging*, 36(2):618–627, 2016.

[58] Yuqi Wang, Haidy G Nasief, Sarah Kohn, Andy Milkowski, Tom Clary, Stephen Barnes, Paul E Barbone, and Timothy J Hall. Three-dimensional ultrasound elasticity imaging on an automated breast volume scanning system. *Ultrasonic imaging*, 39(6):369–392, 2017.

[59] Md Ashikuzzaman and Hassan Rivaz. Denoising rf data via robust principal component analysis: Results in ultrasound elastography. In *2020 42nd Annual*

International Conference of the IEEE Engineering in Medicine & Biology Society (EMBC), pages 2067–2070. IEEE, 2020.

[60] Jingfeng Jiang and Timothy J Hall. A generalized speckle tracking algorithm for ultrasonic strain imaging using dynamic programming. *Ultrasound in medicine & biology*, 35(11):1863–1879, 2009.

[61] Md Ashikuzzaman and Hassan Rivaz. Incorporating multiple observations in global ultrasound elastography. In *2020 42nd Annual International Conference of the IEEE Engineering in Medicine & Biology Society (EMBC)*, pages 2007–2010. IEEE, 2020.

[62] Hassan Rivaz, Emad Boctor, Pezhman Foroughi, Richard Zellars, Gabor Fichtinger, and Gregory Hager. Ultrasound elastography: a dynamic programming approach. *IEEE Trans. Med. Imaging*, 27(10):1373–1377, 2008.

[63] Hoda Sadat Hashemi and Hassan Rivaz. Global time-delay estimation in ultrasound elastography. *IEEE transactions on ultrasonics, ferroelectrics, and frequency control*, 64(10):1625–1636, 2017.

[64] Morteza Mirzaei, Amir Asif, and Hassan Rivaz. Combining total variation regularization with window-based time delay estimation in ultrasound elastography. *IEEE transactions on medical imaging*, 38(12):2744–2754, 2019.

[65] Abdelrahman Zayed and Hassan Rivaz. Fast approximate time-delay estimation in ultrasound elastography using principal component analysis. In *2019 41st Annual International Conference of the IEEE Engineering in Medicine and Biology Society (EMBC)*, pages 6204–6207. IEEE, 2019.

[66] Mohamad Ghasemi Amidabadi, M Omair Ahmad, and Hassan Rivaz. Supervised classification of the accuracy of the time delay estimation in

ultrasound elastography. *IEEE transactions on ultrasonics, ferroelectrics, and frequency control*, 65(1):21–29, 2017.

[67] Zhifan Gao, Sitong Wu, Zhi Liu, Jianwen Luo, Heye Zhang, Mingming Gong, and Shuo Li. Learning the implicit strain reconstruction in ultrasound elastography using privileged information. *Medical image analysis*, 58:101534, 2019.

[68] Sitong Wu, Zhifan Gao, Zhi Liu, Jianwen Luo, Heye Zhang, and Shuo Li. Direct reconstruction of ultrasound elastography using an end-to-end deep neural network. In *International Conference on Medical Image Computing and Computer-Assisted Intervention*, pages 374–382. Springer, 2018.

[69] Abdelrahman Zayed and Hassan Rivaz. Automatic frame selection using mlp neural network in ultrasound elastography. In *International Conference on Image Analysis and Recognition*, pages 462–472. Springer, 2019.

[70] Bo Peng, Yuhong Xian, Quan Zhang, and Jingfeng Jiang. Neural-network-based motion tracking for breast ultrasound strain elastography: An initial assessment of performance and feasibility. *Ultrasonic imaging*, 42(2):74–91, 2020.

[71] Eddy Ilg, Nikolaus Mayer, Tonmoy Saikia, Margret Keuper, Alexey Dosovitskiy, and Thomas Brox. Flownet 2.0: Evolution of optical flow estimation with deep networks. In *IEEE Conference on Computer Vision and Pattern Recognition (CVPR)*, volume 2, 2017.

[72] Deqing Sun, Xiaodong Yang, Ming-Yu Liu, and Jan Kautz. Pwc-net: Cnns for optical flow using pyramid, warping, and cost volume. In *Proceedings of the IEEE conference on computer vision and pattern recognition*, pages 8934–8943, 2018.

[73] Tak-Wai Hui, Xiaoou Tang, and Chen Change Loy. Liteflownet: A lightweight convolutional neural network for optical flow estimation. In *Proceedings of the IEEE conference on computer vision and pattern recognition*, pages 8981–8989, 2018.

[74] Ali KZ Tehrani and Hassan Rivaz. Displacement estimation in ultrasound elastography using pyramidal convolutional neural network. *IEEE Transactions on Ultrasonics, Ferroelectrics, and Frequency Control*, 2020.

[75] Alexey Dosovitskiy, Philipp Fischer, Eddy Ilg, Philip Hausser, Caner Hazirbas, Vladimir Golkov, Patrick van der Smagt, Daniel Cremers, and Thomas Brox. Flownet: Learning optical flow with convolutional networks. In *Proceedings of the IEEE International Conference on Computer Vision*, pages 2758–2766, 2015.

[76] Younsu Kim, Chloé Audigier, Jens Ziegle, Michael Friebe, and Emad M Boctor. Ultrasound thermal monitoring with an external ultrasound source for customized bipolar rf ablation shapes. *IJCARS*, pages 1–12, 2018.

[77] Brage H Amundsen, Thomas Helle-Valle, Thor Edvardsen, Hans Torp, Jonas Crosby, Erik Lyseggen, Asbjørn Støylen, Halfdan Ihlen, João AC Lima, Otto A Smiseth, et al. Noninvasive myocardial strain measurement by speckle tracking echocardiography: validation against sonomicrometry and tagged magnetic resonance imaging. *Journal of the American College of Cardiology*, 47(4):789–793, 2006.

[78] Jonathan Ophir et al. Elastography: Imaging the elastic properties of soft tissues with ultrasound. *J. Med. Ultra.*, 29(4):155–171, 2002.

[79] Cameron Hoerig, Jamshid Ghaboussi, and Michael F Insana. An information-based machine learning approach to elasticity imaging. *Biomech Model Mechanobiol*, 16(3):805–822, 2017.

[80] Jørgen Arendt Jensen. FIELD: A program for simulating ultrasound systems. *Med. Biol. Eng. Comput.*, 34, suppl. 1, pt. 1:351—-353, 1996.

[81] Zhou Wang, Alan C Bovik, Hamid R Sheikh, and Eero P Simoncelli. Image quality assessment: from error visibility to structural similarity. *IEEE TIP*, 13(4):600–612, 2004.

[82] Mina Amiri, Rupert Brooks, and Hassan Rivaz. Fine-tuning u-net for ultrasound image segmentation: Different layers, different outcomes. *IEEE Transactions on Ultrasonics, Ferroelectrics, and Frequency Control*, 67(12):2510–2518, 2020.